Wiley Analytical Science

Wiley Analytical Science Virtual Conference

November 9-17

For the 3rd time, The Wiley Analytical Science Conference is back!

It's all happening November 9 - 17

The Wiley Analytical Science Virtual Conference will bring together thousands of researchers and practitioners to share current developments in science and industry. Join for exciting presentations from experts in the fields of analytical and bioanalytical chemistry, pharmaceutical research, materials science, lab automation, and related disciplines.

Register to learn about recent developments & applications in:

- Microscopy
- Spectroscopy
- Mass Spectrometry
- Separation Science
- Much more!

Register here

WILEY

Predicting the Open-Circuit Voltage of $CH_3NH_3PbI_3$ Perovskite Solar Cells Using Electroluminescence and Photovoltaic Quantum Efficiency Spectra: the Role of Radiative and Non-Radiative Recombination

Wolfgang Tress, Nevena Marinova, Olle Inganäs, Mohammad. K. Nazeeruddin, Shaik M. Zakeeruddin, and Michael Graetzel*

Solar cells based on $CH_3NH_3PbI_3$ perovskites have recently attracted great attention as power-conversion efficiencies have rapidly increased to more than 15%.[1,2] One advantage of this type of solar cell is the versatility of the perovskite deposition, ranging from vapor deposition of flat films in vacuum[2] to solution processing of mesoscopic films by applying several methods.[1,3–7] Different electrode and scaffold layers have been employed and allow for similarly high performance.[8,9] The open-circuit voltage of the best devices is between 1.0 and 1.1 V, which is considered high for a material with a bandgap in the range of 1.5 to 1.6 eV.[8] The reason is seen in a low recombination rate within the solar cells,[10,11] which demands for a quantification and identification of the dominating recombination mechanisms.

In this communication we show that the open-circuit voltage (V_{oc}) of $CH_3NH_3PbI_3$ perovskite solar cells can be theoretically calculated from the reciprocity relation between photovoltaic external quantum efficiency and electroluminescence spectra. We find that charge is photogenerated in the perovskite itself, not requiring any interface with titanium dioxide (TiO_2) or with the hole transport layer. Electrons and holes recombine in the perovskite independently of whether they are photogenerated (photoluminescence) or electrically injected (electroluminescence). Measuring the external electroluminescence yield we explain measured values for V_{oc} and give estimations on the maximum V_{oc} obtainable with $CH_3NH_3PbI_3$ perovskite-based solar cells. We demonstrate that non-radiative surface recombination due to non-selective contacts decreases V_{oc}.

The reciprocity between electroluminescence and photovoltaic quantum efficiency spectra is a fundamental property of several kinds of solar cells.[12] It is a quantification of the postulate stating that a solar cell functions as a light-emitting diode (LED) when charges are injected. This law is a more generalized expression of the equilibrium between absorption and emission,[13–16] which holds generally and determines the maximum energy-conversion efficiency of a solar cell. This is known as the Shockley-Queisser limit describing the case of a single band gap semiconductor where recombination of electron-hole pairs is only radiative.[17] The more generalized form based on the quantum efficiencies allows for an internal quantum efficiency smaller than unity and includes non-radiative recombination. According to this reciprocity relation, only two quantities of a solar cell have to be measured to predict V_{oc}: the photovoltaic quantum efficiency spectrum (EQE_{PV}, also called IPCE) and the external quantum efficiency of the electroluminescence (EQE_{EL}) at V_{oc}.

In the following we briefly sketch how these two quantities determine V_{oc} (for a more elaborated derivation, see ref. [12]: Multiplying the EQE_{PV} with the solar spectrum $\Phi_{AM1.5g}$ expressed as a photon flux and integrating over all wavelengths or equivalently photon energies E yields the photocurrent density J_{ph}, which equals the short-circuit current density (e is the elementary charge):

$$J_{ph} = e\int EQE_{PV}(E)\Phi_{AM1.5g}(E)\mathrm{d}E \quad (1)$$

In the dark, photons are absorbed as well, because the solar cell is in equilibrium (index 0) with the thermal radiation of the surroundings, which is a black body radiation at 300 K (spectral photon flux: $\Phi_{BB}(E) = \frac{1}{4\pi^2\hbar^3c^2}\frac{E^2}{\exp\left(\frac{E}{k_BT_0}\right)-1}$, with Planck's constant $\hbar$, Boltzmann constant k_B, speed of light c, and T_0 = 300 K). The absorbed photon flux has to be reemitted to guarantee equilibrium:

$$J_{abs,0} = e\int a(E)\,\Phi_{BB}(E)\mathrm{d}E = J_{rad,0} \quad (2)$$

Here, $a(E)$ is the absorptance of the solar cell and the overall photon flux is expressed as an equivalent electrical current J. We assume that the emission spectrum does not change for a voltage ≠ 0 and that the semiconductor is in quasi-equilibrium, which allows a definition of quasi-Fermi levels. In this case, the emitted photon flux follows exponentially the splitting of these

Dr. W. Tress, N. Marinova, Dr. M. K. Nazeeruddin, Dr. S. M. Zakeeruddin, Prof. Dr. M. Graetzel
Laboratory of Photonics and Interfaces
Swiss Federal Institute of Technology (EPFL)
Station 6, Lausanne, CH 1015, Switzerland
E-mail: wolfgang.tress@epfl.ch
Dr. W. Tress, Prof. Dr. O. Inganäs
Biomolecular and Organic Electronics
IFM, Linköping University
58183, Linköping, Sweden

DOI: 10.1002/aenm.201400812

levels, i.e., in the ideal case, the voltage measurable at the contacts. The exponential relation can be rationalized with the following idea: Emission is the result of recombination of an electron with a hole. Consequently, the emission probability is proportional to electron and hole density, i.e., the product of both. The electron and hole densities are described by Fermi-Dirac statistics, which can be approximated by a Boltzmann term. Therefore, the electron (hole) density depends exponentially on the difference between Fermi level and conduction (valence) band edge. Hence, we can write for the electrical current giving rise to emission as a function of voltage (V):

$$J_{\mathrm{em}}(V) = J_{\mathrm{rad},0} e^{\frac{eV}{k_B T}} - J_{\mathrm{rad},0} \tag{3}$$

Equation (3) describes the current in the case of the radiative limit. However, in a real device, only a certain fraction of recombination is radiative:

$$J_{\mathrm{em}}(V) = \mathrm{EQE}_{\mathrm{EL}} J_{\mathrm{inj}}(V) \tag{4}$$

If we regard charges being injected by an external voltage source, $\mathrm{EQE}_{\mathrm{EL}}$ can be measured in the dark when the device operates as an LED driven with the injection current $J_{\mathrm{inj}}(V)$. Using Equations (1), (3) and (4) for the injection current, the electrical current under illumination becomes:

$$J(V) = \frac{J_{\mathrm{em},0}}{\mathrm{EQE}_{\mathrm{EL}}}\left(e^{\frac{eV}{k_B T}} - 1\right) - J_{\mathrm{ph}} \tag{5}$$

Setting $J(V)$ to zero yields V_{oc}:

$$V_{\mathrm{oc}} = \frac{k_B T}{e} \ln\left(\mathrm{EQE}_{\mathrm{EL}} \frac{J_{\mathrm{ph}}}{J_{\mathrm{em},0}} + 1\right) \tag{6}$$

As we consider a finite internal quantum efficiency, we replace the absorptance and $J_{\mathrm{rad},0}$ by the $\mathrm{EQE}_{\mathrm{PV}}$ and $J_{\mathrm{em},0}$ according to ref. [12], where $J_{\mathrm{em},0}$ is defined as:

$$J_{\mathrm{em},0} = e \int \mathrm{EQE}_{\mathrm{PV}}(E) \Phi_{\mathrm{BB}}(E) \mathrm{d}E \tag{7}$$

Equation (6) yields in the case of the radiative limit ($\mathrm{EQE}_{\mathrm{EL}} = 1$) for $V_{\mathrm{oc,rad}}$:

$$V_{\mathrm{oc,rad}} = \frac{k_B T}{e} \ln\left(\frac{J_{\mathrm{ph}}}{J_{\mathrm{em},0}} + 1\right) \tag{8}$$

This equation is formally identical to the result obtained from the diode equation although its derivation does not require a pn junction. It is much more general and based on Würfel's generalized Planck law.[18]

According to Equation (6), V_{oc} can be calculated with $\mathrm{EQE}_{\mathrm{EL}}$, $\mathrm{EQE}_{\mathrm{PV}}$, and the temperature of the surroundings assuming thermalized charges.[14] Equation (6) contains the overall $\mathrm{EQE}_{\mathrm{EL}}$ integrated over all wavelengths. Additionally, the principle of detailed balance even requests for the emitted photon flux $\Phi_{\mathrm{em}}(E)$:

$$\Phi_{\mathrm{em}}(E) \propto \mathrm{EQE}_{\mathrm{PV}}(E) \Phi_{\mathrm{BB}}(E) \tag{9}$$

for each E.

Table 1. Characteristic parameters. $J_{\mathrm{em},0}$ is determined according to Equation (7), $V_{\mathrm{oc,rad}}$ according to Equation (8), and $V_{\mathrm{oc,calc}}$ according to Equation (6). J_{sc}, V_{oc}, and $\mathrm{EQE}_{\mathrm{EL}}$ are measured.

	J_{sc} [mA cm^{-2}]	V_{oc} [V]	$J_{\mathrm{em},0}$ [mA cm^{-2}]	$V_{\mathrm{oc,rad}}$ [V]	$\mathrm{EQE}_{\mathrm{EL}}$ at $J_{\mathrm{inj}} = J_{\mathrm{sc}}$	non-rad. loss [V]	$V_{\mathrm{oc,calc}}$ [V]
TiO_2	20	1.01	9×10^{-22}	1.33	2×10^{-6}	0.34	0.99
Al_2O_3	19	1.02	1×10^{-21}	1.32	1×10^{-5}	0.30	1.02
no HTL	11	0.77	3×10^{-22}	1.34	8×10^{-10}	0.54	0.80

In the following we apply the derived equations to perovskite solar cells comparing three different devices: i) a "standard" TiO_2 based one, consisting of glass/fluorine doped tin oxide/TiO_2 compact layer (50 nm)/TiO_2 mesoporous layer (250 nm)/perovskite (infiltrated)/doped spiro-MeO-TAD (infiltrated plus 100 nm capping layer)/Au (80 nm).[1] ii) The same as the first one, but with the scaffold interchanged with an aluminum oxide Al_2O_3 mesoporous layer. iii) The same as the first one, but without hole-transport layer (HTL). Thus, the perovskite is in direct contact with the gold electrode.

Table 1 contains the characteristic parameters of those solar cells (J–V curves in the Supporting Information). Data of average-performance devices were chosen as the focus is not on the highest efficiency. The error is not explicitly mentioned but variations from device to device and between different measurements are in the range of 5%. The devices with Al_2O_3 and TiO_2 scaffold perform similarly (V_{oc} = 1.0 V and J_{sc} = (19 ± 1) mA cm^{-2}). However, short-circuit current density and open-circuit voltage are significantly lower for the device without HTL. V_{oc} of all devices was stable in the error range during the measurements themselves (timespan of hours) and while storing them under low pressure between different measurements (weeks).

To calculate $J_{\mathrm{em},0}$ according to Equation (7), we need to know the $\mathrm{EQE}_{\mathrm{PV}}$. As Φ_{BB}(300 K) is an exponentially decaying function in the visible spectral range, a precise measurement of the $\mathrm{EQE}_{\mathrm{PV}}$ onset is important. Here, we use a Fourier-transform based photocurrent spectroscopy technique (FTPS) delivering data with a high sensitivity.[19] FTPS spectra are shown in the inset of **Figure 1** as solid lines. They are scaled to match the $\mathrm{EQE}_{\mathrm{PV}}$ obtained from a calibrated setup (dotted). This setup provides the absolute EQE spectrum, however, with insufficient sensitivity to investigate the onset on a logarithmic scale. The more sensitive FTPS spectra are shown on a logarithmic scale in the main part of the figure and normalized at 1.8 eV for a better comparability of the onset. The spectra roughly coincide showing a sharp onset as seen for the absorbance.[20]

There is no significant difference between TiO_2 and Al_2O_3. This indicates that the signal is only from the perovskite. The interface between TiO_2 and perovskite does not allow for any detectable optical transitions in contrast to what is observed at a donor-acceptor interface in an organic solar cell. There, charge-transfer states are generated, which describe a direct optical transition between the two different molecular materials.[19] The differences in the onset of few meV are in between sample-to-sample variations. Consequently, the maximum of V_{oc} is not governed by the interface to the contact material, but by the perovskite itself. The signal for devices without HTL is lower (see inset) as both the internal quantum efficiency and

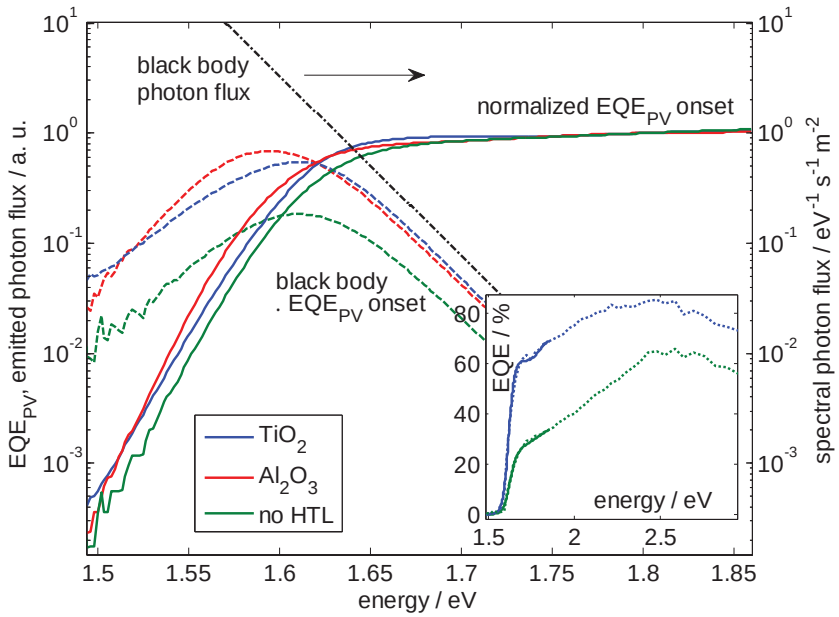

Figure 1. Onset of the incident-photon-to-electron-conversion efficiency (EQE_{PV}) measured with Fourier-transform photocurrent spectroscopy and normalized at 1.8 eV (lines). Shown are data for devices with TiO_2 or Al_2O_3 scaffold and for one device without hole-transport layer. Dashed is the calculated emitted spectral photon flux when the device is in equilibrium with the black-body radiation of the surroundings (dash-dotted). The inset compares the EQE_{PV} onset from FTPS with the overall EQE_{PV} measured with monochromatic light and a lock-in amplifier. The EQE_{PV} of the device without HTL is lower due to optical and electrical losses, whereas the EQE_{PV} for Al_2O_3 and TiO_2 devices with HTL are comparable.

the reflectivity of the (then rough) gold electrode are less if it is penetrating the active layer (Supporting Information).

According to Equation (9) we can calculate the emitted photon flux spectrum knowing the $EQE_{PV}(E)$ or vice versa.[14,16] These spectra (dashed lines) are added to the figure together with the black body radiation expressed as a photon flux at 300 K (dash-dotted). The emission intensity becomes less for an absorption onset shifted towards higher energies due to the decay of $\Phi_{BB}(300\ K)$ with energy.

To check whether the reciprocity relations hold, we investigate EL and $EQE_{PV}(E)$ of a TiO_2 device in more detail with the aid of **Figure 2**. The EL data were recorded at an applied voltage in the range of 1 to 2 V (1 to 10 mA, selected here are 5 mA). The spectra do not change shape with applied voltage (see Supporting Information) in contrast to what is observed in amorphous organic materials.[21] Consequently, the radiative recombination channel is independent of voltage, which indicates that disorder does not play a role and that charges are in quasi-equilibrium within their energy bands.

The graph shows that experimental and calculated photon flux spectra (Equation (9)) are very close (peak at 1.60 eV). Thus, the observed electroluminescence radiation results from an electron and a hole being injected into the perovskite, meeting each other inside the bulk, and recombining directly. This result is in accordance with reports showing the ambipolarity of the perovskite.[4,22] We can deduce the temperature of the material (or more precisely of the charge carriers) during the EL experiment from the slope in the exponential plot. Comparing the measured data with the theoretical line for 320 K, we observe a good fit. This number is realistic and indicates a slight heating of the material during current flow. We also performed the reciprocal calculation using

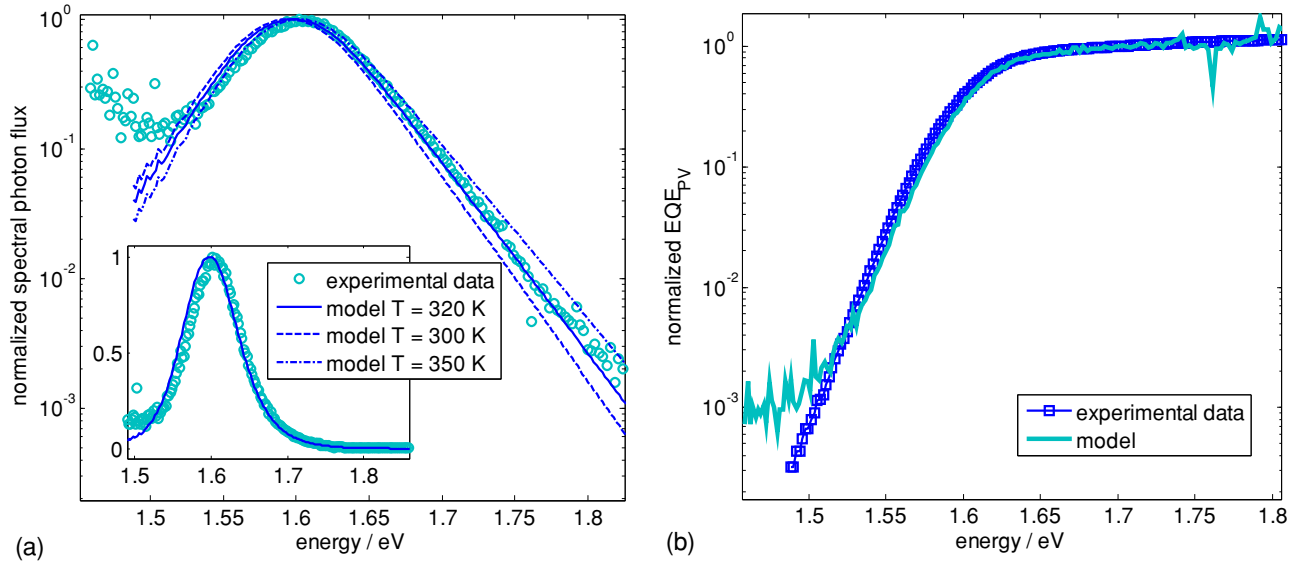

Figure 2. a) Normalized electroluminescence photon flux spectrum: measured data (symbols) and spectra predicted from EQE_{PV} assuming different temperatures, where a temperature of ≈320 K is found to fit the experiment best. The limit of the detector is at 1.5 eV. b) Measured EQE_{PV} compared to the spectrum modeled based on the experimental EL data. The model data fit well in the range of detection of the EL. The spectral resolution is in the range of few meV.

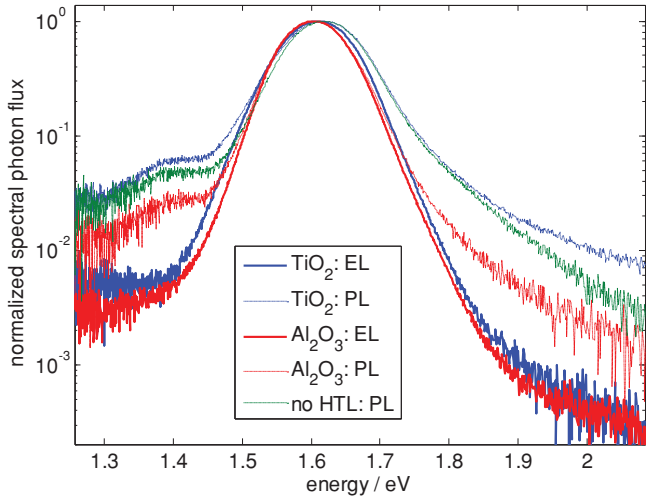

Figure 3. Electroluminescence (EL) and photoluminescence (PL) emission spectra as a function of photon energy. Overall, PL and EL peak coincide. Additionally, the PL shows a weak broad parasitic signal from the substrate. The spectral resolution is in the range of 5 meV.

Equation (9). From the measured EL spectrum we deduce the EQE_{PV} onset, which works remarkably well as demonstrated in Figure 2b. Thus, we can predict the open-circuit voltage for state-of-the-art perovskite devices using EQE_{PV}.

To check whether the emission spectra differ when investigating injected or photogenerated charges, we compare EL with photoluminescence (PL) in **Figure 3**. We observe that the peak is at the same position. Consequently, the PL and EL share the same origin, i.e., recombination of free electron-hole pairs in the perovskite. The PL is not a parasitic signal. It can be quenched in magnitude when going from open circuit to short circuit or even applying a negative bias (Supporting Information). This implies that the PL at V_{oc} (partly) originates from charges, which contribute to photocurrent at voltages below V_{oc}. The PL shows additional signal compared to the EL, in particular for devices with TiO_2 scaffold. The additional broad weak PL is not seen at pure perovskite films. It results mainly from impurities in the glass/FTO substrate and is enhanced due to scattering of the mesoscopic TiO_2 film. Also impurities or oxygen vacancies[23] in TiO_2 itself might play a role. This signal is less quenched with applied negative voltage, but is reduced as well (Supporting Information).

Knowing $J_{em,0}$ and J_{ph} we can calculate the theoretical, i.e., radiative, limit of V_{oc} (Equation (8)). More precisely, only the ratio between J_{ph} and $J_{em,0}$ is required, which can be obtained even without knowing the absolute EQE_{PV} but only the shape. The calculated value, added to the data in Table 1, is between 1.32 V and 1.34 V and is given by the perovskite, but not by the device architecture. The trend follows the shift of the onset of the absorption, and reflects rather a sample-to-sample variation than a systematic difference with respect to the sample stack. It is highest for the device without HTL due to the slightly shifted absorption and the relatively low signal of the EQE_{PV} close to the onset decreasing $J_{em,0}$ in Equation (7), but a less reduced J_{ph} due to a large EQE_{PV} for higher energies. A V_{oc} of (1.33 ± 0.02) V would be predicted by the Shockley Queisser limit for a band-edge absorber (absorptance 1 for energies larger than the band gap, else 0) with a band gap of 1.59 to 1.63 eV.

Obviously, the measured open-circuit voltage is much lower than the theoretical maximum. This reduction is due to non-radiative recombination. We can quantify non-radiative recombination by measuring the emission yield (EQE_{EL}) of the EL spectra, which we have shown only as normalized data so far. The emitted spectral photon flux integrated over all wavelengths and divided by the injection current is depicted as a function of the injection current in **Figure 4**. It approaches values close to 10^{-4}, which is large compared to common values for organic solar cells ranging from 10^{-9} to 10^{-6}.[19] Whereas the difference between the EQE_{EL} for the Al_2O_3 and TiO_2 based devices is in the range of device-to-device variations, it is much lower for the device without HTL. The reason is that for the device without HTL the injection current is driven by electrons through the perovskite, which recombine non-radiatively at the perovskite/gold interface providing a non-selective contact.[24]

Interestingly, the EQE_{EL} depends strongly on the injection current. To calculate V_{oc} we should take the value, where the injection current equals the photocurrent (Equation (6)). There, the EQE_{EL} is in the range of 2×10^{-6} for the TiO_2-based device, 1×10^{-5} for the Al_2O_3-based device and three orders of

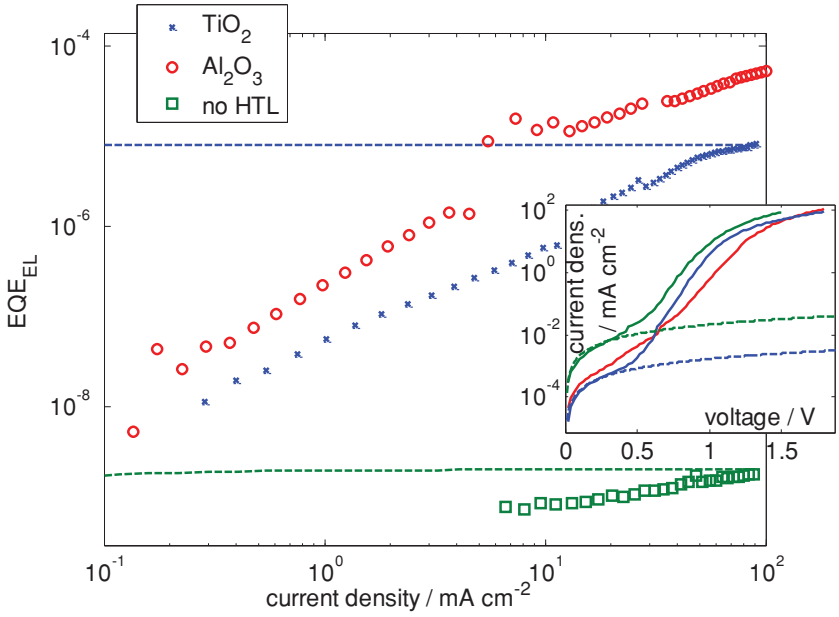

Figure 4. External electroluminescence yield (EQE_{EL}) as a function of the injection current. Dashed lines show the calculated EQE_{EL} assuming that its measured dependence on voltage is only due to a shunt, which is obviously not the case for the experimental data. The injection current as a function of applied voltage is shown in the inset (solid lines) including a fit to a shunt resistance (dashed), which is used to calculate the dashed lines in the main figure. Due to slight changes of the current–voltage relation, instability of the devices at high forward bias, and the setup, the EQE_{EL} at a fixed voltage point might vary by a factor of two.

magnitude lower for the device without HTL. The values are added to Table 1, together with the calculated V_{oc} according to Equation (6), which fits the measured one well including the difference between devices with and without HTL. Discrepancies are due to the fact that the *J–V* curves of the devices do not behave ideally in a way that the *J–V* curve under illumination is the *J–V* curve in the dark minus a constant photocurrent. Consequently, the current–voltage point, where the injection current compensates for J_{ph}, is not at open circuit and less defined.

Figure 4 shows that the EQE_{EL} (i.e., share of radiative recombination) increases with injection current by several orders of magnitude. Thus, there are non-radiative recombination paths that dominate at low currents. These might be partial shunts, surface recombination due to non-perfectly selective contacts, or non-radiative recombination in the active material itself due to recombination via trap or tail states. Looking at the *J–V* curves (inset), the influence of shunts is rather seen for voltages smaller than 0.5 V. We can calculate the EQE_{EL} assuming that its dependence on current results from a shunt only: $EQE'_{EL}(V) = EQE_{EL,const} \times J_{diode}(V)/(J_{shunt}(V) + J_{diode}(V))$. The calculated $EQE'_{EL}(V)$ is shown for two devices as dashed lines in Figure 4, where $EQE_{EL,const}$ is chosen as the value measured at high voltages and the shunt is derived from a fit to the *J–V* curve for voltages below 0.3 V. Obviously, the shunt cannot explain the magnitude of the observed changes in EQE_{EL}.

The traces of high recombination at the contact can be seen at the device without HTL, which does not show a strong dependence of EQE_{EL} on injection current. Consequently, we exclude recombination at the contact as a major source of the strong dependence of EQE_{EL} on injection current for the devices with HTL. In turn, we conclude that the non-radiative recombination results from the perovskite mesoscopic layer itself. The increase of the emission yield with current indicates that non-radiative recombination is only possible through a limited number of states. Consequently, it is expected to be further suppressed by passivation measures, avoiding trap states, etc. First studies on adding passivation molecules have already shown slight improvements of V_{oc}.[25] This result is promising and implies that reported values of V_{oc} are not the limit. As theoretical studies do not predict intrinsic trap states (such as vacancies) acting as recombination centers in the material,[26] the source of non-radiative recombination is most likely due to dislocations, grain boundaries, impurities, or PbI_2 that is not fully converted into perovskite. Auger-type recombination does not limit V_{oc} for state-of-the-art devices, as it is a three-particle process, which becomes significant only for higher injection currents. This would lead to a decrease of EQE_{EL} with injection current. However, the opposite is observed. Thus, optimizing the perovskite morphology and device architecture, e.g., by reducing the thickness of the absorber while maintaining high photocurrents are keys to increase V_{oc}. Selective contacts are a prerequisite for highly efficient devices, where doped spiro-MeO-TAD seems to work already relatively well. Further studies are necessary to reveal the prevailing recombination mechanism(s) in microcrystalline perovskite films in more detail.

In conclusion we have shown that the open-circuit voltage of perovskite solar cells is described by the general reciprocity between electroluminescent emission and photovoltaic action. Both are governed by the perovskite as an ambipolar semiconductor where electrons and holes are photogenerated and (injected) electrons and holes recombine. The limit for V_{oc} in case of solely radiative recombination is determined as 1.32 to 1.34 V. Non-radiative losses at V_{oc} are found to be relatively low, but still decrease this value to around 1.0 V for average state-of-the-art devices and even below if contacts are not selective. The strong increase of the electroluminescence emission yield with injection current indicates that a better passivation and reduction of non-radiative losses within the mesoporous multicrystalline perovskite layer will allow for highly efficient devices with voltages possibly exceeding 1.1 V.

Experimental Section

Device Preparation: Devices were fabricated on clean fluorine-doped tin oxide coated glass (NSG). A blocking layer of compact TiO_2 was deposited by spin coating of precursor 2 M water solution of $TiCl_4$ at 5000 rpm for 20 s and dried at 70 °C. The mesoporous TiO_2 and Al_2O_3 layers were formed by spin coating of colloidal solutions of TiO_2 and Al_2O_3 with particle size of 20 and 22.6 nm respectively, at 5000 rpm for 20 s. The films were then gradually heated to 500 °C and sintered at that temperature for 15 min. 1 M lead iodide DMF solution was spin coated onto the mesoporous TiO_2 at 6500 rpm for 30 s and dried at 70 °C. After drying the deposition of lead iodide was repeated in order to ensure a better loading of the mesoporous structure with lead iodide. The perovskite layer was formed after dipping the substrate into CH_3NH_3I solution in isopropanol (10 mg mL^{-1}) for 30 s, followed by rinsing with isopropanol, and drying at 70 °C. For the devices with HTL a solution of 72.3 g Spiro MeOTAD in 1 mL chlorobenzene was prepared, containing 10 mol% FK 209, 28.8 µL tert-butylpyridine and 17.5 µL solution of lithium bis(trifluoromethylsulfonyl)imide (Li-TFSI 520 mg mL^{-1} in acetonitrile). The HTL solution was spin coated onto the perovskite surface at 4000 rpm for 30 s. The device architecture was completed with 80 nm gold counter electrode, which was thermally evaporated on top of the device.

Spectroscopy: FTPS measurements were performed using a Vertex 70 FT-IR Spectrometer from Bruker, which is operated at external detector option. PL and EL were collected with a light guide positioned close to the devices. The detector was a Newton EM-CCD Si array detector at –60 °C with a Shamrock sr 303i spectrograph from Andor Tech. For the PL, a green laser (532 nm, 5 mW, spot size few mm^2) was used as excitation source; for the EL, the voltage was applied with a Keithley 2400 SMU. Additional EL experiments were performed using a Fluorolog spectrofluorometer from Horiba. The EQE_{EL} was detected measuring the emitted photon current with a calibrated large-area Si-photodetector positioned close to the sample.

Supporting Information

Supporting Information is available from the Wiley Online Library or from the author.

Acknowledgements

The authors thank Kunwu Fu for EL measurements. W.T. and O.I. kindly acknowledge support by the Knut and Alice Wallenberg foundation (Sweden). The authors acknowledge funding from the European Union Seventh Framework Program [FP7/2007–2013] under grant agreement n° 604032 of the MESO project, M.G. thanks the European Research Council (ERC) for financial support under the advanced research grant (ARG 247404) "Mesolight".

Received: May 15, 2014
Revised: September 8, 2014
Published online: September 30, 2014

[1] J. Burschka, N. Pellet, S.-J. Moon, R. Humphry-Baker, P. Gao, M. K. Nazeeruddin, M. Grätzel, *Nature* **2013**, *499*, 316.
[2] M. Liu, M. B. Johnston, H. J. Snaith, *Nature* **2013**, *501*, 395.
[3] A. Yella, L.-P. Heiniger, P. Gao, M. K. Nazeeruddin, M. Grätzel, *Nano Lett.* **2014**, *14*, 2591.
[4] J. M. Ball, M. M. Lee, A. Hey, H. J. Snaith, *Energy Environ. Sci.* **2013**, *6*, 1739.
[5] M. J. Carnie, C. Charbonneau, M. L. Davies, J. Troughton, T. M. Watson, K. Wojciechowski, H. Snaith, D. A. Worsley, *Chem. Commun.* **2013**, *49*, 7893.
[6] Q. Chen, H. Zhou, Z. Hong, S. Luo, H.-S. Duan, H.-H. Wang, Y. Liu, G. Li, Y. Yang, *J. Am. Chem. Soc.* **2014**, *136*, 622.
[7] J. You, Z. Hong, Y. (Michael) Yang, Q. Chen, M. Cai, T.-B. Song, C.-C. Chen, S. Lu, Y. Liu, H. Zhou, Y. Yang, *ACS Nano* **2014**, *8*, 1674.
[8] H.-S. Kim, C.-R. Lee, J.-H. Im, K.-B. Lee, T. Moehl, A. Marchioro, S.-J. Moon, R. Humphry-Baker, J.-H. Yum, J. E. Moser, M. Grätzel, N.-G. Park, *Sci. Rep.* **2012**, *2*.
[9] M. M. Lee, J. Teuscher, T. Miyasaka, T. N. Murakami, H. J. Snaith, *Science* **2012**, *338*, 643.
[10] C. S. Ponseca, T. J. Savenije, M. Abdellah, K. Zheng, A. Yartsev, T. Pascher, T. Harlang, P. Chabera, T. Pullerits, A. Stepanov, J.-P. Wolf, V. Sundström, *J. Am. Chem. Soc.* **2014**, *136*, 5189.
[11] F. Deschler, M. Price, S. Pathak, L. E. Klintberg, D.-D. Jarausch, R. Higler, S. Hüttner, T. Leijtens, S. D. Stranks, H. J. Snaith, M. Atatüre, R. T. Phillips, R. H. Friend, *J. Phys. Chem. Lett.* **2014**, *5*, 1421.
[12] U. Rau, *Phys. Rev. B* **2007**, *76*, 085303.
[13] G. Kirchhoff, *Ann. Phys.* **1860**, *185*, 275.
[14] G. Smestad, H. Ries, *Sol. Energy Mater. Sol. Cells* **1992**, *25*, 51.
[15] T. Trupke, E. Daub, P. Würfel, *Sol. Energy Mater. Sol. Cells* **1998**, *53*, 103.
[16] T. Trupke, P. Würfel, I. Uhlendorf, I. Lauermann, *J. Phys. Chem. B* **1999**, *103*, 1905.
[17] W. Shockley, H. J. Queisser, *J. Appl. Phys.* **2004**, *32*, 510.
[18] P. Wurfel, *J. Phys. C Solid State Phys.* **1982**, *15*, 3967.
[19] K. Vandewal, K. Tvingstedt, A. Gadisa, O. Inganäs, J. V. Manca, *Nat. Mater.* **2009**, *8*, 904.
[20] S. De Wolf, J. Holovsky, S.-J. Moon, P. Löper, B. Niesen, M. Ledinsky, F.-J. Haug, J.-H. Yum, C. Ballif, *J. Phys. Chem. Lett.* **2014**, *5*, 1035 .
[21] K. Tvingstedt, K. Vandewal, A. Gadisa, F. Zhang, J. Manca, O. Inganäs, *J. Am. Chem. Soc.* **2009**, *131*, 11819.
[22] G. Xing, N. Mathews, S. Sun, S. S. Lim, Y. M. Lam, M. Grätzel, S. Mhaisalkar, T. C. Sum, *Science* **2013**, *342*, 344.
[23] F. Montoncello, M. C. Carotta, B. Cavicchi, M. Ferroni, A. Giberti, V. Guidi, C. Malagù, G. Martinelli, F. Meinardi, *J. Appl. Phys.* **2003**, *94*, 1501.
[24] E. J. Juarez-Perez, M. Wuβler, F. Fabregat-Santiago, K. Lakus-Wollny, E. Mankel, T. Mayer, W. Jaegermann, I. Mora-Sero, *J. Phys. Chem. Lett.* **2014**, 680.
[25] A. Abate, M. Saliba, D. J. Hollman, S. D. Stranks, K. Wojciechowski, R. Avolio, G. Grancini, A. Petrozza, H. J. Snaith, *Nano Lett.* **2014**, *14*, 3247.
[26] J. Kim, S.-H. Lee, J. H. Lee, K.-H. Hong, *J. Phys. Chem. Lett.* **2014**, *5*, 1312.